ADVANCED FUNCTIONAL MATERIALS
www.afm-journal.de

Pressure Sensing and Electronic Amplification with Functionalized Graphite–Silicone Composite

Samuel Littlejohn, Alain Nogaret, Giles M. Prentice, and G. Dan Pantos*

A flexible yet electronically active composite that mimics mechanoreceptor neurons in the human skin is synthesized, generating voltage oscillations whose frequency increases with pressure. By encoding pressure into frequency, the sensor achieves a high pressure sensitivity (<10 Pa). The ability to sense pressure and to amplify signals arises from the robust negative differential resistance of functionalized graphitic flakes in silicone.

1. Introduction

The need for flexible electronics that fit curved surfaces or moving parts is driving the search for conformable conducting materials.[1–4] Flexible skins that incorporate electromechanical,[5,6] thermal[7] and optical sensors[8–10] have been obtained. However, the pursuit of mechanoreceptors that approach the sensitivity of the human skin remains an enduring challenge.[11–15] In the natural world, the sense of touch is implemented by nerve terminals that convert pressure into sustained electric oscillations achieving, in this way, immunity to noise and accurate readout of a pressure stimulus whose intensity is encoded in the pulse frequency. Here, we report an electronically active composite capable of generating spontaneous voltage oscillations which, like sensory neurons in the human skin, oscillate at a frequency that increases with mechanical strain. The composite was synthesized by admixing functionalized graphite nanoparticles in silicone resulting in strain sensors which are flexible, biocompatible, and which sense strain with high accuracy (<10 Pa). The composite exhibits a robust negative differential resistance (NDR) region at low temperature (T < 200 K) which supports spontaneous voltage oscillations and amplifies a.c. signals with a gain tuneable between 1 and 5. The spontaneous oscillations are found to combine two pure modes: a driven mode (<8 kHz) and a natural mode whose frequency depends on strain (2.0 kHz–3.5 kHz). The latter oscillations are found to arise from positive feedback amplification in the percolation network. The results demonstrate graphite–silicone composites as an electronically active material that could be used for making pressure sensitive skins.

S. Littlejohn, Dr. A. Nogaret
Department of Physics
University of Bath
Claverton Down, Bath BA2 7AY, UK
E-mail: A.R.Nogaret@bath.ac.uk
G. M. Prentice, Dr. G. D. Pantos
Department of Chemistry
University of Bath
Claverton Down, Bath BA2 7AY, UK

DOI: 10.1002/adfm.201300519

2. Results and Discussion

Composites were prepared by mixing 450 nm highly ordered pyrolytic graphite (HOPG) nanoparticles in liquid silicone. The mixture was cast at the surface of 100 μm thick cellulose acetate sheets and cured at room temperature to obtain 100 μm thick, 1 mm wide ribbons. Pristine HOPG nanoparticles are miscible in silicone up to a volume fraction of p = 32% where clustering begins. To bring the NDR region to lower bias and reduce Joule heating to stabilize voltage oscillations, we have coated the surface of HOPG nanoparticles with naphthalenediimide (NDI) molecules[16–18] (**Figure 1** a) functionalized with three types of side chains: 1) –Si–OR (NDI–Si), 2) -2-ethylhexyl (NDI–Hex), 3) 2,2-diphenylethyl (NDI–Ph) (Figure 1b). The extended aromatic core of NDI–Si adheres to the graphite surface via π–π interactions while the Si–OR end-groups are covalently bound to the –(–Si–O)$_n$– polymeric chains of the silicone rubber matrix. This effective interfacial vulcanization overcomes the hydrophobic barrier of the graphite surface with the effect of lowering the silicone–HOPG potential barrier. This can be seen in Figure 1c and Supporting Information, Section I, where NDI–Si functionalization reduces the resistance of the composite by a factor of 2 relative to control samples prepared with the same HOPG filling fraction. NDI–Si also gives significantly resistance compared to NDI–Hex and NDI–Ph functionalizations (Figure 1c). A second advantage of NDI–Si functionalization is that it further increases the miscibility of HOPG nanoparticles in silicone from 32% to 39%. This corresponds to the average tunnelling barrier width being reduced from 80 nm to 46 nm with a four orders of magnitude increase in tunnelling current.[19] Having identified NDI–Si as the best functionalization agent, we proceed to study NDI–Si composites with a filling fraction p = 36% to increase conductivity and move the peak current to low bias voltage: 15–25 V. A scanning electron microscope (SEM) image of the composite (Figure 1d) shows the lamellar structure of HOPG nanoparticles. The angular distribution of graphite planes is isotropic, which accounts for the random nature of the mixing process.

The conductive paths percolate through the composite by tunnelling from one HOPG node to the next via silicone potential barriers.[19] The composite exhibits a wide and robust NDR region that occurs through the break-down of the π-band in HOPG. Graphite is known to have anisotropic conductivity $\sigma_{\parallel}/\sigma_{\perp} \approx 3000$ that favors conduction in the plane of the layers.[20] If, however, graphite planes are tilted by a large angle relative to the electric field, the current injected in one layer will hop into a neighbouring layer before exiting the particle. The

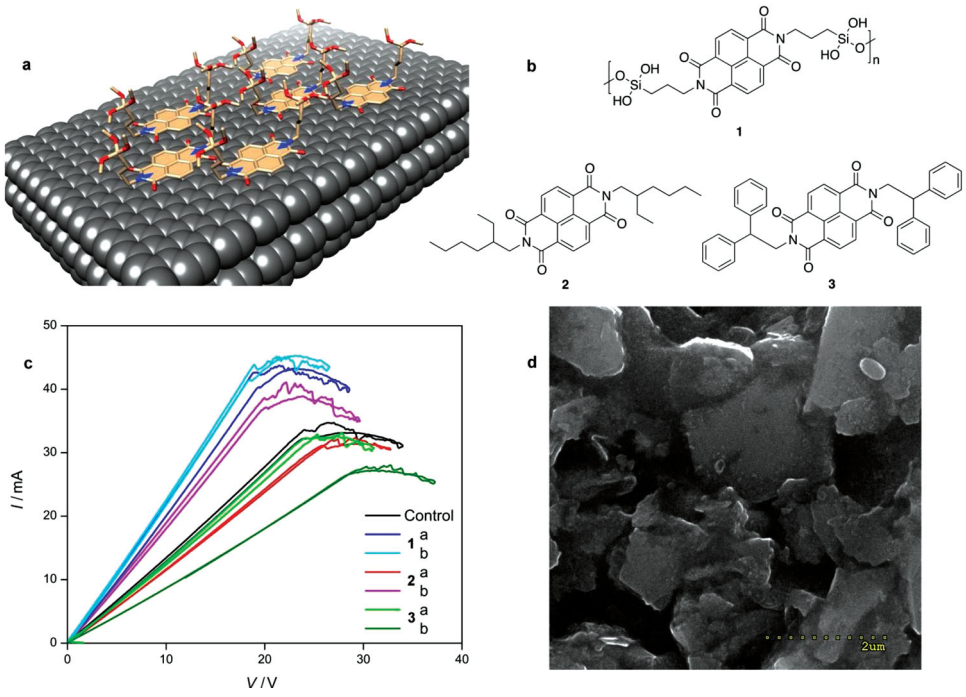

Figure 1. Graphite-silicone composite. a) Naphthalenediimide molecules at the surface of a HOPG nanoparticle. The extended aromatic core of the molecule adheres to the graphite surface while the –Si–OR appendages anchor the polymerized chains of silicone rubber. b) Naphthalene diimide molecules with three different side chains were used to functionalize HOPG nanoparticles: 1) NDI–Si ($C_{26}H_{34}N_2O_{10}Si_2$, molecular weight: 590.73), 2) NDI–Hex ($C_{30}H_{38}N_2O_4$, molecular weight: 490.63), 3) NDI–Ph ($C_{42}H_{30}N_2O_4$, molecular weight: 626.70). c) The current–voltage characteristics of the composite film exhibit a peak followed by a wide NDR region ($T = 77$ K). The current–voltage curves compare the effect of the functionalization by the 3 types of NDI molecules with a control sample that remained unfunctionalized. The HOPG filling fraction ($p = 36\%$) is the same for all 3 samples however series (a) and (b) have 50% and 500% nominal NDI coverage respectively. d) SEM image of the composite. This reveals a random distribution of faceted HOPG particles of average size 450 nm.

critical angle for bilayer conduction is $\theta_c = \arctan\left(\frac{\sigma_{||}}{\sigma_\perp}\frac{c}{d}\right)$ where $c = 0.337$ nm is the interlayer separation and d is the particle size. We find $\theta_c = 66°$ for our HOPG particles ($d = 450$ nm). It follows that particles tilted at an angle $\theta > \theta_c$ in the composite are the weak links in the percolation path(s). The electric field being localized to one graphene bilayer, a moderate bias (100 mV) across the particle is sufficient to break the π-band of graphite.[19,21,22] The particle undergoes a metal-insulator transition which shuts down the percolation path. The electrically induced metal-to-insulator transition of graphite nanoparticles has been shown to cause the NDR[19,23,24] observed in Figure 1b. In-situ temperature measurements show that the low temperature NDR is not a result of Joule heating (Supporting Information, Section II). This is further confirmed by the observation of spontaneous voltage oscillations in the NDR region at frequencies much higher than the thermal relaxation rate in the composite (see below).

The composite/acetate bilayer was mounted between clamps and bent into an arc by compressive force applied to its edges (**Figure 2**a). Curving the strip upwards or downwards places the composite under tensile ($\varepsilon > 0$, where ε is the differential strain) or compressive strain ($\varepsilon < 0$). Once bent, the sample was cooled to 77 K and its current–voltage characteristics (I–V) were recorded. To change the bend radius, the sample was thermally cycled to room temperature. The I–V curves remained remarkably resilient and reproducible after the composite was subjected to both thermal and bend cycles (Supporting Information, Section III). Placing the composite under increasing strain was found to increase the differential resistance R_{lin} in the both linear part of the I–V curve and in the NDR region (Figure 2a). The same trend was observed under tension and compression.[1]

To evaluate ε at the interface between the composite and the substrate, we have computed the curvature radius ρ of the bilayer as a function of the horizontal deformation $\eta = \frac{l_0 - l}{l_0}$ where l_0 is the length of the flat strip and l is the chord of its arc when bent. The theoretical dependence of ρ on η (Figure 2b, black line) is in good agreement with the experimental data (Figure 2b, black squares). This justifies inserting the $\rho(\eta)$ formula in the ρ-dependence of the differential strain[25] $\rho(\varepsilon)$ (Supporting Information, Section IV) to obtain the following relationship between strain ε and horizontal deformation η:

$$\varepsilon(\eta) = \frac{h}{l_0}\left(14 + \frac{E_1}{E_2} + \frac{E_2}{E_1}\right)\sqrt{\frac{\eta}{24}} \quad (1)$$

$E_1 \approx 4$ MPa and $E_2 \approx 400$ MPa are the Young's moduli of the composite and acetate respectively; $h = 200$ nm is the thickness of the strip. Equation 1 is plotted in Figure 2b (red line). The experimental data points (red dots) are obtained by assuming a linear dependence between $\delta R_{\text{lin}}/R_{\text{lin}}$ and ε via the piezoresistive constant, π_{lin}. We find the $\delta R/R(\eta)$ dependence fits the calculated $\varepsilon(\eta)$ dependence best for $\pi_{\text{L}} = 2.6 \pm 0.2$.

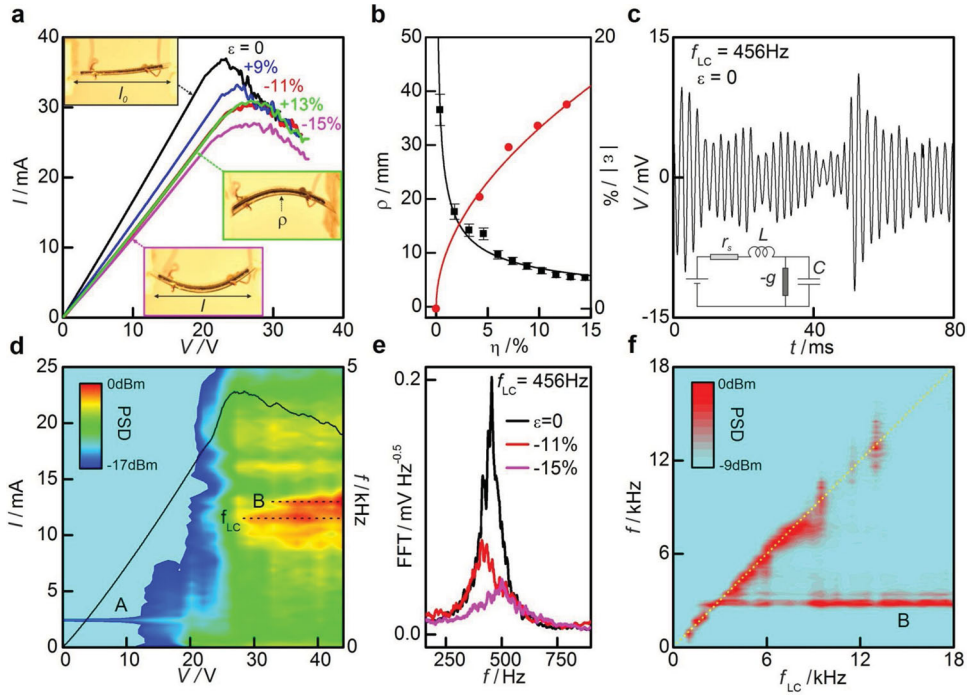

Figure 2. Flexible oscillators. a) *I–V* curves of a thin composite film under tensile ($\varepsilon > 0$) and compressive strain ($\varepsilon < 0$) measured using a four-probe technique. b) Curvature radius ρ of the composite/acetate strip deformed by horizontal compression $\eta = (l_0 - l)/l_0$: experimental (black squares), theory (full black line); differential strain ε at the graphite/acetate boundary: experimental (red dots), theory (full red line). c) A composite film oscillates spontaneously when it is incorporated in a tuned circuit (inset) and biased in the NDR region. The resonant frequency of the tuned circuit is f_{LC} = 456 Hz and V = 25 V. d) Power spectral density of the tuned composite oscillator mapped as a function of the bias voltage over the range of the *I–V* curve (full line). Spontaneous voltage oscillations start in the NDR region and have maximum amplitude at the resonant frequency f_{LC}. Lines A (450 Hz) and B (2500 Hz) are the natural oscillation frequencies of the composite. e) Spectrum of spontaneous oscillations and its dependence on compressive strain. f) Power spectral density of spontaneous oscillations mapped as a function of f_{LC}. L = 2.2 mH, $r_s \approx 150\ \Omega$, g = 0.8 mS. f_{LC} is tuned with variable capacitor C.

The composite device was then embedded in a tuned resonator circuit (inset, Figure 2c) and biased in the NDR region to demonstrate the generation of spontaneous oscillations by the flexible material. Given that the negative differential conductance was $g \approx 0.8$ mS and the resistance of the contacts was r_s = 150 Ω, the stability condition for the composite to oscillate, $g\ r_s < 1$, is fulfilled.[26] We show that the composite indeed oscillates when biased in the NDR region (Figure 2c). The oscillation frequency, f = 456 Hz, matches the resonant frequency $f_{LC} = \frac{1}{2\pi}\sqrt{\frac{1}{LC} - \frac{g^2}{C^2}}$ of the *LC* circuit. The oscillation amplitude generally fluctuates over time due to nonlinearities in the system. These oscillations become most regular when f_{LC} crosses one of the natural frequencies of the composite in which case the oscillation amplitude stabilizes. By increasing the series resistance r_s we verify that the oscillations vanish when $r_s \approx 1/g$. We also verify that spontaneous oscillations only appear in the NDR region. This is shown in the dependence of the power spectral density on the bias voltage (Figure 2d). When $V < V_p$, the composite does not oscillate. At V > V_p the a.c. power surges rapidly and saturates in the NDR region. The main emission line is centred at f_{LC} however two subsidiary lines: A (450 Hz) and B (2.2 kHz) are also found which are the natural frequencies of the composite. The Fourier spectrum of the time series data shows a sharp resonance at f_{LC} (Figure 2e). The amplitude of this resonance decreases under strain.

Next, we study the power spectral density as a function of f_{LC} to determine the emission bandwidth of the oscillator (Figure 2f). To this end, we swept the frequency of the *LC* circuit f_{LC} by steadily decreasing the value of capacitor C while keeping the value of the inductor constant L = 2.2 mH. We find that the composite behaves as an active source that generates a.c. power up to a maximum frequency $f_r = \frac{g}{2\pi C_r}\sqrt{\frac{1}{gr_s} - 1}$. This frequency is reached when $C = C_r = gL/r_s$ (Supporting Information, Section V) at which point the oscillation frequency does not increase anymore and becomes independent of C. In Figure 2f, this saturation is seen at f = 7.8 kHz. These observations suggest the existence of a capacitance intrinsic to the composite, C_c, that comes to dominate the oscillator response when C becomes very small. By writing that the two capacitances are equal at the cut-off, one obtains C_c = 220 nF. This is the intrinsic capacitance of the composite which sets the upper frequency limit of the oscillator.

To study oscillations under strain, we substitute a larger inductor L = 47 mH so that f_r remains below the intrinsic saturation frequency at f = 7.8 kHz. As strain increases from ε = 0 to ε = 14%, the frequency bandwidth of tuned oscillations increases from 600 Hz to 2.2 kHz (**Figure 3**a–e, red diagonal). This increase in cut-off frequency is due to $f_r \propto g^{-1/2}$ and g decreasing with increasing strain. To prove this dependency, we calculate f_r using the negative differential conductances, g,

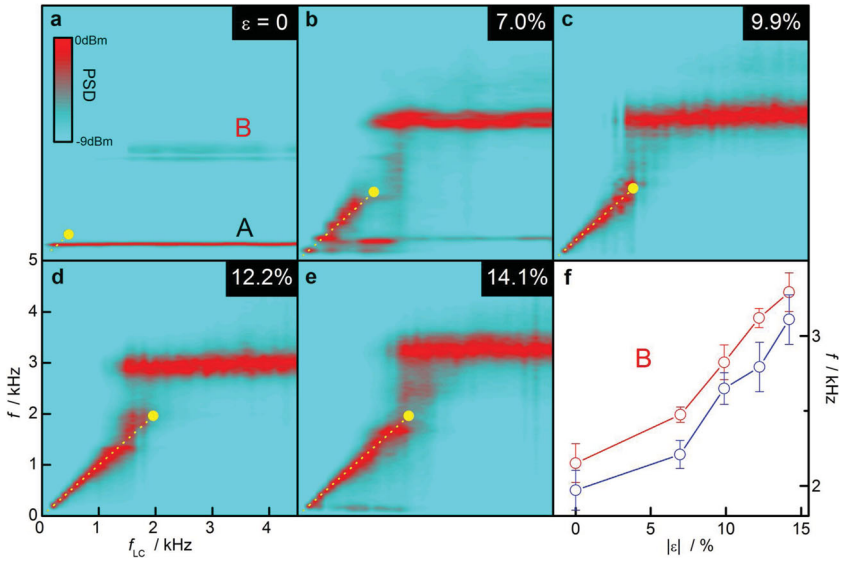

Figure 3. Strain dependence of spontaneous oscillations at 77 K. a–e) Power spectral density of the composite film bent at increasingly tight curvature radii. The effect of increasing the compressive strain is to increase the cut-off frequency of the tuned oscillations (yellow dot) and to increase the natural frequencies A and B of the composite (horizontal red lines). The theoretical dependence of the tuned frequency (yellow dashed line) is shown with the experimental dependence (diagonal red branch). The theoretical cut-off frequency (yellow dot) was calculated using L = 47 mH, $r_s \approx 130\ \Omega$ and the $-g$ values obtained from each I–V curve under strain. f) Strain dependence of resonance B extracted from panels (a–e) (red circles) and obtained from another nominally similar sample (blue circles) to demonstrate reproducibility.

taken from the I–V curves at different values of the applied strain (Supporting Information, Figure S6). The theoretical cut-offs (yellow dots, Figure 3a–e) are in very good agreement with the experimental cut-offs. Figure 3 thus demonstrates a plastic oscillator with tuneable bandwidth. Now turning to the natural oscillations of the composite, resonances A and B occur at frequencies which are independent of both C (Figure 3b) and L but depend strongly on strain (Figure 3a–e). These oscillations occur even after the LC resonator has been removed. The natural oscillations, like the tuned oscillations, are only observed in the NDR region. Under strain, resonance B shifts from 2150 Hz at $\varepsilon = 0$ to 3330Hz at $\varepsilon = 14\%$ which represents an average rate of increase of $\lambda = 84$ Hz/% strain (Figure 3f). The natural oscillations can be explained with a percolation model of the composite in which the total applied bias is dropped across a manifold of tunnelling barriers of varying widths. Thermodynamic considerations require that under constant bias voltage, the equilibrium potential profile is the one that maximizes the conductivity of the network. Departures from this equilibrium, caused by, for example, charge accumulation in one cell, would decrease the overall conductivity as a change of bias in the opposite direction in another cell would be required to keep the total voltage constant. We argue that at the site of cells involving the $\theta > 66°$ HOPG nanoparticles responsible for the NDR, these fluctuations are self-sustaining. Transient charge accumulation ($\Delta Q\uparrow$) in one such particle will increase capacitive bias in the adjacent silicone barrier ($\Delta V\uparrow$). As the cell is biased in the NDR region the current decreases ($\Delta I\downarrow$). This in turn reduces charge accumulation ($\Delta Q\downarrow$) and, hence, the local bias ($\Delta V\downarrow$). However, the cell remains biased in the NDR region, causing the current to increase again ($\Delta I\uparrow$) and charge accumulation to resume ($\Delta Q\uparrow$). A positive feedback loop of this kind propelled by the NDR can explain the self-sustained natural oscillations. The effect of strain here is to decrease the amplitude of current oscillations $|\Delta I| = |g| \times |\Delta V|$ since $|g|$ decreases when the composite is bent (Supporting Information, Figure S6). This effect is experimentally observed in the Fourier spectrum of Figure 2e. Under strain, smaller deflections from equilibrium $|\Delta I|$ will also give faster oscillations by reducing nonlinear inertia. This picture explains the increase in oscillation frequency observed under both tensile and compressive strain since in both cases $|g|$ decreases (Figure 3a–e). The strain dependence of natural oscillations, as a new physical effect, is valuable for making skin-like transducers that encode strain into frequency. The rate of change of frequency with strain is:

$$\frac{\Delta f}{\Delta P} = \frac{\lambda}{E_1} = 2.1\ \mathrm{mHz/Pa} \qquad (2)$$

The accuracy of the sensor will only be limited by the width of the integration time window. A window of 1 s gives an uncertainty on frequency of Δf = 1 Hz hence a pressure sensitivity of ΔP = 475 Pa. A time window of 60 s would increase the pressure sensitivity to ΔP = 8 Pa.

Finally, we have built a tuned voltage amplifier that uses composite films as the active element (**Figure 4**). The typical time series data of the amplified signal are shown in Figure 4a. We

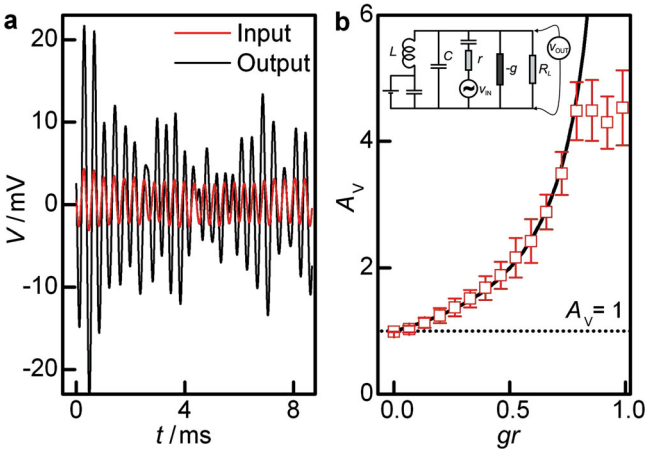

Figure 4. Flexible amplifier. a) Time series data of the input and output voltages of a tuned NDR amplifier showing an average gain of 2. The amplifier incorporates a thin composite film as the active element. b) Inset: tuned voltage amplifier. The voltage gain $A_v = 1/(1-gr)$ is controlled by resistor r and the negative differential conductance of the composite $-g$. Main panel: the dependence of the experimental gain (squares) and the theoretical gain (full line) on r. L = 47 mH, C = 680 nF, R_L = 1 MΩ, $g \approx 0.8$ mS.

are able to control the voltage gain between 1 and 5 using the resistance r of the amplifier circuit (inset to Figure 4b). This is because the voltage gain is $A_v = \frac{1}{1-gr}$ at the resonant frequency (Supporting Information, Section VI). The experimental gain (averaged over 25 oscillations) is plotted as a function of r in Figure 4b (squares) and compared to the theoretical gain (full line). These results demonstrate graphite–silicone composites as a flexible material capable of electronic amplification.

3. Conclusions

We have made the first flexible amplifier and oscillator using graphite–silicone composites which are cheap, scalable, and biocompatible. The composite is shown to encode strain through frequency modulation, mimicking tactile receptors in the skin and lending itself for use as an artificial skin.

4. Experimental Section

Graphite–silicone composites were prepared by first mixing 450 nm HOPG nanoparticles (Nanoamor) with NDI functionalization agents in proportions calculated to give 50% and 500% NDI coverage of HOPG nanoparticles—see samples series (a) and (b) in Figure 1c. The nominal NDI coverage was evaluated using the coverage formula in Supporting Information, Section I. The NDI/HOPG weight ratios for each individual sample are given in Figure S3, Supporting Information. The functionalized HOPG nanoparticles were then mixed in liquid silicone (Alchemie, RTV139) and catalyst (Alchemie C149) in the weight ratios given in Figure S3 of the Supporting Information to achieve a nominal HOPG volume filling fraction of 36%. HOPG nanoparticles were dispersed in liquid silicone using mortar and pestle grinding over a longer time than that required for the mixture to become homogeneous. The composite was moulded in the form of 1 mm wide ribbons at the surface of cellulose acetate films. The film thickness was 100 ± 8 μm. The composite was left to cure at room temperature for 24 h. Gold pads (50 nm thick) were thermally evaporated over the composite ribbon giving good Ohmic contacts with ≈100 Ω resistance.

Supporting Information

Supporting Information is available from the Wiley Online Library or from the author.

Received: February 8, 2013
Revised: April 20, 2013
Published online: May 31, 2013

[1] J. A. Rogers, T. Someya, Y. Huang, *Science* **2010**, *327*, 1603.
[2] C. Wang, J.-C. Chien, K. Takei, T. Takahashi, J. Nah, A. M. Kijnejad, A. Javey, *Nano Lett.* **2012**, *12*, 1527.
[3] Z. Chen, W. Ren, L. Gao, B. Liu, S. Pei, H.-M. Cheng, *Nat. Mater.* **2011**, *10*, 424.
[4] S. Stankovich, D. A. Dikin, G. H. B. Dommett, K. M. Kohlhass, E. J. Zimmey, E. A. Stach, R. D. Piner, S. T. Nguyen, R. Ruoff, *Nature* **2006**, *442*, 283.
[5] T. Someya, T. Sekitani, S. Iba, Y. Kato, H. Kawaguchi, T. Sakurai, *Proc. Natl. Acad. Sci. USA* **2004**, *101*, 9966.
[6] L. Chen, G. Chen, L. Lu, *Adv. Funct. Mater.* **2007**, *17*, 898.
[7] T. Someya, Y. Kato, T. Sekitani, S. Iba, Y. Noguchi, Y. Murase, H. Kawaguchi, T. Sakurai, *Proc. Natl. Acad. Sci. USA* **2004**, *102*, 12321.
[8] M. S. Humayun, J. D. Weiland, G. Y. Fujii, R. Greenberg, R. Williamson, J. Little, B. Mech, V. Cimmarusti, G. Van Boemel, G. Dagnelie, E. De Juan Jr., *Vision Res.* **2003**, *43*, 2573.
[9] H. Sirringhaus, N. Tessler, R. Friend, *Science* **1998**, *280*, 1741.
[10] T. Sekitani, H. Nakajima, H. Maeda, T. Fukushima, T. Aida, K. Hata, T. Someya, *Nat. Mater.* **2009**, *8*, 494.
[11] J. Boland, *Nat. Mater.* **2010**, *9*, 790.
[12] M. Gad El Hak, *Act. Flow. Control* **2007**, *95*, 1.
[13] H. Klauk, U. Zschieschang, J. Pflaum, M. Halik, *Nature* **2007**, *445*, 745.
[14] T. Sekitani, U. Zschieschang, H. Klauk, T. Someya, *Nat. Mater.* **2010**, *9*, 1015.
[15] M. Ying, A. P. Bonifas, N. Lu, Y. Su, R. Li, H. Cheng, A. Ameen, Y. Huang, J. A. Rogers, *Nanotechnology* **2012**, *23*, 344004.
[16] P. Pengo, G. D. Pantos, S. Otto, J. K. M. Sanders, *J. Org. Chem.* **2006**, *71*, 7063.
[17] L. Kleiner-Shuhler, R. Brittain, M. R. Johnston, K. W. J. Hipps, *J. Phys. Chem. C* **2008**, *112*, 14907.
[18] Z. Hu, G. D. Pantos, N. Kuganathan, R. L. Arrowsmith, R. M. J. Jacobs, G. Kociok-Köhn, J. O'Byrne, K. Jurkschat, P. Burgos, R. M. Tyrrell, S. W. Botchway, J. K. M. Sanders, S. I. Pascu, *Adv. Funct. Mater.* **2012**, *22*, 503.
[19] S. Littlejohn, A. Nogaret, S. Crampin, *Adv. Mater.* **2011**, *23*, 2815.
[20] M. S. Dresselhaus, G. Dresselhaus, *Adv. Phys.* **2002**, *51*, 1.
[21] E. McCann, V. I. Fal'ko, *Phys. Rev. Lett.* **2006**, *96*, 086805.
[22] T. Ohta, A. Bostwick, T. Seyller, K. Horn, E. Rotemberg, *Science* **2006**, *313*, 951.
[23] K. M. M. Habib, F. Zahid, R. K. Lake, *Appl. Phys. Lett.* **2011**, *98*, 192112.
[24] R. Nandkishore, L. Levitov, *Proc. Natl. Acad. Sci. USA* **2011**, *108*, 14021.
[25] S. Timoshenko, *J. Opt. Soc. Am.* **1925**, *11*, 233.
[26] W. F. Chow, *Principles of tunnel diode circuits*, Wiley, New York **1964**.